



The Interacting Multiple Model Algorithm for Accurate State Estimation of Maneuvering Targets

Anthony F. Genovese

Accurate state estimation of targets with changing dynamics can be achieved through the use of multiple filter models. The interacting multiple model (IMM) algorithm provides a structure to efficiently manage multiple filter models. Design of an IMM requires selection of the number and type of filter models and selection of each of the individual filter parameters. In this article the results for five filter models on 10 target trajectory segments are discussed and compared. The complexity of the filter models increases from a single constant velocity model to a three-model IMM filter. The results show that the overall performance of the state estimates, for most targets, improves as the complexity of the filter models increases. Selection of IMM filter parameters is addressed and results are provided to show that performance of the IMM appears to be relatively insensitive to large changes in filter parameters. The performance of an IMM is primarily determined by the selection of the component filter models.

INTRODUCTION

The performance of a tracking system is governed by the performance of the state estimation algorithm employed. Accurate state estimation of targets in a tracking system is required for reliable data association and correlation. The states to be estimated are typically the kinematic quantities of position, velocity, and acceleration. Filters are used on measurements to reduce the uncertainty due to noise on the observation and to estimate quantities not directly observed. The filter uses a model of the state process that can be used to accurately predict the behavior of the observed target to estimate the desired kinematic quantities.

State estimation of potentially maneuvering targets from sensor measurements often requires the use of

multiple filter models to account for varying target behavior. Efficient management of the multiple filter models is critical to limiting algorithm computations while achieving the desired tracking performance. This requirement is achieved with the interacting multiple model (IMM) algorithm.¹

The IMM algorithm is a method for combining state hypotheses from multiple filter models to get a better state estimate of targets with changing dynamics. The filter models used in the IMM for each state hypothesis can be selected to match the behavior of targets of interest. Model management for the IMM algorithm is governed by an underlying Markov chain that controls the switching behavior among the multiple models. For the

resulting algorithm, logic decisions are not required for estimation of the model probabilities.^{2,3}

BACKGROUND

State estimation for tracking is most effectively done by modeling the target trajectory as a linear system. The discrete-time state representation of a linear system is given in the following equation:

$$\mathbf{X}_{k+1} = \Phi_k \mathbf{X}_k + \mathbf{w}_k,$$

where \mathbf{X}_k is the state estimate, Φ_k is a state transition matrix from time k to $k+1$, and \mathbf{w}_k is system process noise assumed to be Gaussian-distributed zero mean and white.

Observations for this process are assumed to be linear with respect to the state estimate. The observations are then given as

$$\mathbf{y}_k = \mathbf{H}_k \mathbf{X}_k + \mathbf{v}_k,$$

where \mathbf{H}_k is the matrix relating the state to observation quantities and \mathbf{v}_k is observation noise assumed to be Gaussian-distributed zero mean and having zero cross correlation with the process noise \mathbf{w}_k .

The Kalman filter provides the minimum mean squared error solution to this linear system problem when the process under observation is completely represented by the state model.⁴ The equations used to predict and update the state and covariance for a Kalman filter are given as follows:

$$\begin{aligned} \hat{\mathbf{X}} &= \Phi \hat{\mathbf{X}} \\ \hat{\mathbf{P}} &= \Phi \hat{\mathbf{P}} \Phi^T + \mathbf{Q} \\ \mathbf{K} &= \hat{\mathbf{P}} \mathbf{H}^T (\mathbf{H} \hat{\mathbf{P}} \mathbf{H}^T + \mathbf{R})^{-1} \\ \hat{\mathbf{X}} &= \hat{\mathbf{X}} + \mathbf{K} (\mathbf{y}_k - \mathbf{H} \hat{\mathbf{X}}) \\ \hat{\mathbf{P}} &= (\mathbf{I} - \mathbf{K} \mathbf{H}) \hat{\mathbf{P}}, \end{aligned}$$

where

- \mathbf{X} = the state estimate,
- \mathbf{P} = the covariance matrix,
- $\sim, \hat{}$ = the predicted and filtered quantities, respectively,
- Φ = the discrete time state transition matrix,
- \mathbf{Q} = the process noise matrix,
- \mathbf{K} = the Kalman gain,
- \mathbf{R} = the covariance of the measurement quantity,
- \mathbf{I} = an identity matrix,
- \mathbf{y}_k = the measurement quantity used to update the state estimate, and
- \mathbf{T} = the matrix transpose operation.

Most tracking systems employ a single filter model with adaptive gains for state estimation of maneuvering

targets. These systems require the detection of the target maneuver via a second estimator and decision-directed logic to change gains. The problems with this system are that the decision to switch can be delayed as a result of lags in the maneuver detection filter and false alarms can give false maneuver indications. In addition, a single state estimator will exhibit biases when the model is not matched to the target motion.

Multiple filter models enable a tracking system to better match changing target dynamics. This will yield the best overall performance on the maneuvering and nonmaneuvering time intervals of targets. The effective application of multiple models requires an algorithm to manage the models. Desired performance must be weighed against system resources. The IMM algorithm has been shown to be a very efficient implementation of the multiple model approach.¹

The IMM Algorithm

The IMM algorithm is a method for combining state hypotheses from multiple filter models to get a better state estimate of targets with changing dynamics. The filter models used to form each state hypothesis can be derived to match the behavior of targets of interest. Figure 1 shows the flow diagram for an IMM algorithm with two filter models. Superscripts in the state variables represent the model hypotheses (1 and 2), and the symbols $\hat{}$ and \sim are used to represent filtered and predicted quantities, respectively.

The state estimates for each model from the previous cycle, $\hat{\mathbf{X}}^1$ and $\hat{\mathbf{X}}^2$, are mixed prior to state update using a set of conditional model probabilities. The conditional model probabilities ($\tilde{\mu}^{ij}$) are computed using the model probabilities from the previous update and a

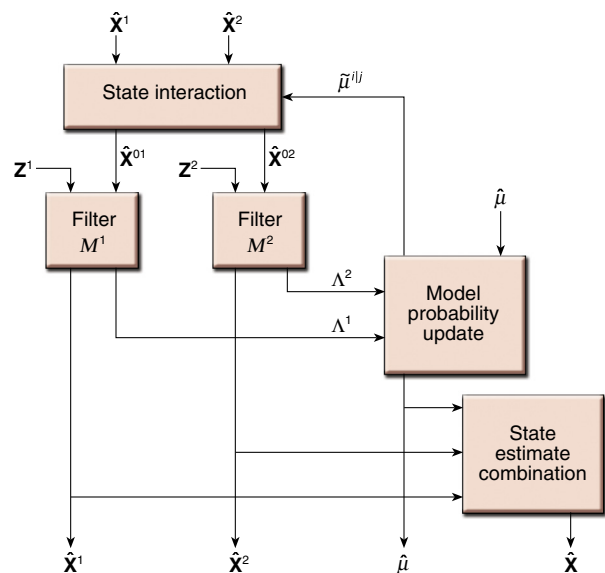


Figure 1. A block diagram of the IMM algorithm with two filter models.

state switching matrix selected *a priori*. The mixed state estimates are updated using each filter model. The likelihood (Λ^i) for each filter model is computed during the state update from the innovations (\mathbf{Z}^i) and innovations covariance matrix. The likelihood, prior model probabilities, and state switching matrix are then used to update the model probabilities. The estimates from each filter model are combined as a weighted sum using the updated model probabilities.

The equations governing the IMM algorithm for an arbitrary number of filter models, N , are outlined in the following steps. The process then begins with the computed quantities from the previous filter iteration. Initialization procedures are required to obtain the state estimate, covariance, and initial probabilities for each filter model.

State Interaction

Prior to the filter update, the model state estimates and covariances are mixed using computed conditional model probabilities. The mixed state and covariance for model j at time k is computed as

$$\hat{\mathbf{X}}^{0j} = \sum_{i=1}^N \hat{\mathbf{X}}^i \tilde{\mu}^{ij}$$

and

$$\hat{\mathbf{P}}^{0j} = \sum_{i=1}^N \tilde{\mu}^{ij} \left[\hat{\mathbf{P}}^i + (\hat{\mathbf{X}}^i - \hat{\mathbf{X}}^{0j})(\hat{\mathbf{X}}^i - \hat{\mathbf{X}}^{0j})^T \right],$$

where

$$\tilde{\mu}^{ij} = \frac{1}{\bar{\Psi}^j} p^{ij} \hat{\mu}^i$$

with

$$\bar{\Psi}^j = \sum_{i=1}^N p^{ij} \mu^i,$$

where p^{ij} is the ij element of the state switching matrix ($\mathbf{\Pi}$) that defines the *a priori* probability for switching from model i to model j , and $\bar{\mathbf{c}}^j$ is a normalization vector used to maintain a total model probability of 1. Also note that $\hat{\mathbf{X}}^{0j}$ is the mixed state estimate for each filter model and $\hat{\mathbf{P}}^{0j}$ is the mixed state covariance.

Model Probability Update

The likelihood of each model is computed using the innovations \mathbf{Z}^j computed during state update and the innovations covariance matrix $\tilde{\mathbf{S}}^j$ computed in the Kalman gain. This step is done after state prediction of each mixed state estimate. If Gaussian statistics are assumed, the likelihood of model j is given by

$$\Lambda^j = \frac{1}{\sqrt{|2\pi\tilde{\mathbf{S}}^j|}} \exp\left[-0.5(\mathbf{Z}^j)^T(\tilde{\mathbf{S}}^j)^{-1}(\mathbf{Z}^j)\right],$$

where

$$\begin{aligned} \mathbf{Z}^j &= \mathbf{m}_o - \tilde{\mathbf{m}}^j \\ \tilde{\mathbf{S}}^j &= \mathbf{H}^j \mathbf{P}^{0j} (\mathbf{H}^j)^T + \mathbf{R}, \end{aligned}$$

where \mathbf{m}_o is a vector of observations for the current update and $\tilde{\mathbf{m}}^j$ is the predicted track state for filter model j transformed into the frame of the observations.

The model probabilities are updated after all filter models have been updated as

$$\hat{\mu}^j = \frac{1}{c} \Lambda^j \bar{\mathbf{c}}^j$$

with

$$c = \sum_{i=1}^N \Lambda^i \bar{\mathbf{c}}^i,$$

where $\hat{\mu}^j$ is the updated model probability for model j and c is a normalization constant. Note that innovations covariance matrix $\tilde{\mathbf{S}}^j$ is computed using the predicted covariance matrix $\hat{\mathbf{P}}^{0j}$.

State Estimate Combination

The combined state estimate and covariance is computed from the updated filtered states from each model weighted by the updated model probabilities:

$$\hat{\mathbf{X}} = \sum_{i=1}^N \hat{\mathbf{X}}^i \hat{\mu}^i$$

and

$$\hat{\mathbf{P}} = \sum_{i=1}^N \hat{\mu}^i \left[\hat{\mathbf{P}}^i + (\hat{\mathbf{X}}^i - \hat{\mathbf{X}})(\hat{\mathbf{X}}^i - \hat{\mathbf{X}})^T \right].$$

FILTER MODEL DEFINITIONS

Three filter models have been selected to test the IMM algorithm with different configurations. These models are a constant velocity (CV), a constant acceleration (CA), and a three-dimensional turn with a kinematic constraint (TURN).

CV Model

The state vector for the CV filter model is defined as

$$\mathbf{X} = [x \ \dot{x} \ y \ \dot{y} \ z \ \dot{z}]^T,$$

where x corresponds to the east component, y corresponds to the north component, z corresponds to the zenith component, and \dot{x} , \dot{y} , and \dot{z} are the corresponding rates. Target accelerations are modeled as a continuous-time white noise process to ensure model stability. This model will yield the best estimates of position and velocity on nonmaneuvering targets. The extended Kalman filter derived in Ref. 5 is used as the basis for the CV filter model.

The state transition matrix for the CV model is defined for a linear prediction from the track valid time to the time of the measurements

$$\Phi = \begin{bmatrix} \bar{\varphi}_{CV} & \mathbf{0}_2 & \mathbf{0}_2 \\ \mathbf{0}_2 & \bar{\varphi}_{CV} & \mathbf{0}_2 \\ \mathbf{0}_2 & \mathbf{0}_2 & \bar{\varphi}_{CV} \end{bmatrix},$$

where

$$\bar{\varphi}_{CV} = \begin{bmatrix} 1 & \Delta t \\ 0 & 1 \end{bmatrix} \quad \text{and} \quad \mathbf{0}_2 = \begin{bmatrix} 0 & 0 \\ 0 & 0 \end{bmatrix},$$

and where Δt is the difference of the measurement time and valid time of the track.

The plant noise matrix for the CV filter model is derived as the discrete time representation of the white noise acceleration. This matrix is given as

$$\mathbf{Q} = \begin{bmatrix} \bar{q}_{CV} & \mathbf{0}_2 & \mathbf{0}_2 \\ \mathbf{0}_2 & \bar{q}_{CV} & \mathbf{0}_2 \\ \mathbf{0}_2 & \mathbf{0}_2 & \bar{q}_{CV} \end{bmatrix},$$

where

$$\bar{q}_{CV} = q\Delta t \begin{bmatrix} \frac{\Delta t^2}{3} & \frac{\Delta t}{2} \\ \frac{\Delta t}{2} & 1 \end{bmatrix}.$$

The parameter q is the filter plant noise spectral density and has units of m^2/s^3 . This parameter is selected to control the steady-state gain performance of the filter.

CA Model

The filter state vector for the CA filter model is defined as

$$\mathbf{X} = [x \ \dot{x} \ \ddot{x} \ y \ \dot{y} \ \ddot{y} \ z \ \dot{z} \ \ddot{z}]^T,$$

where the position and rate terms are the same as those in the CV model and \ddot{x} , \ddot{y} , and \ddot{z} are the acceleration estimates.

The state transition matrix is defined for a linear prediction in all three dimensions using all state estimate terms

$$\Phi = \begin{bmatrix} \bar{\varphi}_{CA} & \mathbf{0}_3 & \mathbf{0}_3 \\ \mathbf{0}_3 & \bar{\varphi}_{CA} & \mathbf{0}_3 \\ \mathbf{0}_3 & \mathbf{0}_3 & \bar{\varphi}_{CA} \end{bmatrix},$$

where

$$\bar{\varphi}_{CA} = \begin{bmatrix} 1 & \Delta t & \Delta t^2/2 \\ 0 & 1 & \Delta t \\ 0 & 0 & 1 \end{bmatrix} \quad \text{and} \quad \mathbf{0}_3 = \begin{bmatrix} 0 & 0 & 0 \\ 0 & 0 & 0 \\ 0 & 0 & 0 \end{bmatrix}.$$

The plant noise matrix is defined as

$$\mathbf{Q} = \begin{bmatrix} \bar{q}_{CA} & \mathbf{0}_3 & \mathbf{0}_3 \\ \mathbf{0}_3 & \bar{q}_{CA} & \mathbf{0}_3 \\ \mathbf{0}_3 & \mathbf{0}_3 & \bar{q}_{CA} \end{bmatrix},$$

where

$$\bar{q}_{CA} = q\Delta t \begin{bmatrix} 0 & 0 & 0 \\ 0 & 0 & 0 \\ 0 & 0 & 1 \end{bmatrix}.$$

The parameter q for this model has units of m^2/s^5 . The prediction and process noise model for this filter is derived in Ref. 6.

TURN Model

The filter state vector for the TURN filter model is the same as that for the CA model,

$$\mathbf{X} = [x \ \dot{x} \ \ddot{x} \ y \ \dot{y} \ \ddot{y} \ z \ \dot{z} \ \ddot{z}]^T.$$

The state transition matrix for this model is defined to perform a constant-speed turn maneuver along the trajectory defined by the state estimates of velocity and acceleration. This matrix is given as

$$\Phi = \begin{bmatrix} \bar{\varphi}_{TURN} & \mathbf{0}_3 & \mathbf{0}_3 \\ \mathbf{0}_3 & \bar{\varphi}_{TURN} & \mathbf{0}_3 \\ \mathbf{0}_3 & \mathbf{0}_3 & \bar{\varphi}_{TURN} \end{bmatrix},$$

where

$$\bar{\varphi}_{TURN} = \begin{bmatrix} 1 & \omega^{-1} \sin(\omega\Delta\tau) & \omega^{-2}(1 - \cos(\omega\Delta\tau)) \\ 0 & \cos(\omega\Delta\tau) & \omega^{-1} \sin(\omega\Delta\tau) \\ 0 & -\omega \sin(\omega\Delta\tau) & \cos(\omega\Delta\tau) \end{bmatrix},$$

and ω is the turning rate calculated from elements of the filtered track state as

$$\omega = \frac{\|\bar{\mathbf{A}}\|}{\|\bar{\mathbf{V}}\|} = \frac{\sqrt{\dot{x}^2 + \dot{y}^2 + \dot{z}^2}}{\sqrt{\ddot{x}^2 + \ddot{y}^2 + \ddot{z}^2}}.$$

The plant noise matrix for this model is the same as for the CA model.

The TURN model also uses a pseudo-measurement update derived from the constraint that the target is undergoing a constant-speed turning maneuver. Using the pseudo-measurement derived from this maneuver assumption tends to influence the state estimates to change to fit the profile of this type of target. Namely, the vector representation of the acceleration estimate will change to be normal to the velocity vector. Application of this pseudo-measurement will also affect the filter model covariance, with the result that the covariance is smaller than true measurement noise-only errors. However, lag errors are significantly reduced during the turn period using this procedure. The full derivation of this procedure is given in Ref. 7, and the filter model is applied within an IMM structure in Ref. 8.

The constraint is applied as a pseudo-measurement update to the TURN model. The filtering equations for this formation have been derived as

$$\hat{v}^c = \frac{1}{\|\hat{v}\|} [00 \dot{x} 00 \dot{y} 00 \dot{z}]$$

$$K^c = \hat{P}\hat{v}^T[\hat{v}\hat{P}\hat{v}^T + R^c]^{-1}$$

$$\hat{X} = [I - K^c\hat{v}]\hat{X}$$

$$\hat{P} = [I - K^c\hat{v}]\hat{P}$$

where the superscript *c* in each equation denotes terms related to the pseudo-measurement update. **R^c** is the variance of the pseudo-measurement update selected for this application to achieve a gain of 0.5. In the IMM filter model this constraint is applied twice: once after state interaction and once after the measurement update for the TURN filter model.

FILTER MODELS FOR PERFORMANCE COMPARISON

A study has been conducted to compare the performance of five filtering methods. The application considered is tracking of airborne targets. The filtered root mean square (RMS) position and velocity errors have been compared on a variety of maneuvering targets. The five filtering methods with operating parameters are given in Table 1.

The five filter models have been selected to show filter performance as a function of increasing filter complexity. The first two methods are single filter methods,

Table 1. Filtering methods for comparison study.

Method	Filter models	Filter parameters	
1	CV	$q_{CV} = 400 \text{ m}^2/\text{s}^3$	
2	CA	$q_{CA} = 400 \text{ m}^2/\text{s}^5$	
3	CV-CV IMM	$q_{CV} = 1 \text{ m}^2/\text{s}^3$ $q_{CA} = 3600 \text{ m}^2/\text{s}^3$	$\mathbf{\Pi} = \begin{bmatrix} 0.95 & 0.05 \\ 0.12 & 0.88 \end{bmatrix}$
4	CV-CA IMM	$q_{CV} = 1 \text{ m}^2/\text{s}^3$ $q_{CA} = 400 \text{ m}^2/\text{s}^5$	
5	CV-CA-TURN IMM	$q_{CV} = 1 \text{ m}^2/\text{s}^3$ $q_{CA} = 400 \text{ m}^2/\text{s}^5$ $q_{TURN} = 25 \text{ m}^2/\text{s}^5$	$\mathbf{\Pi} = \begin{bmatrix} 0.90 & 0.08 & 0.02 \\ 0.15 & 0.70 & 0.15 \\ 0.04 & 0.16 & 0.80 \end{bmatrix}$

and the last three are IMM filters. Methods 1 and 2 will show filter model performance for nonadaptive single model filters. The CV filter *q* value for method 1 was selected high in order to reasonably limit lags during target maneuvers. The CA filter *q* value was selected the same for all filter methods where a CA model is used. The three IMM methods represent an increase in complexity that should be reflected in the results. The filter parameters were selected experimentally using general guidelines. Filter parameter selection and its impact on the IMM filter performance will be addressed later in this article.

Two sensor models are selected to provide a broader view of the filter performance as applied under different operating conditions. The first sensor is a surveillance (scan) radar that provides detections at a 4-s update period. The second is a high-precision (HP) radar with an update period of 1 s. Each sensor model provides three-dimensional measurements of position that are zero-mean and Gaussian. The standard deviation of measurement noise for each sensor model is given in Table 2.

The two sensor models are used in combination with five maneuvering target models to provide a testing suite for the filter models. The five maneuvering target models are a weaving maneuver with a 12-s weave period, 10-g linear speed acceleration for 10 s, high-altitude 6-g dive, 1-g constant speed turn, and 5.6-g constant speed turn.

Table 2. Sensor model parameters.

	Scan	High precision
Update period (s)	4	1
Range accuracy (m)	50	5
Bearing accuracy (Mrad)	5	1
Elevation accuracy (Mrad)	5	1

RESULTS

The simulation results for each filter model are obtained from Monte Carlo simulations with 100 realizations. The RMS errors for position and velocity are computed from the filtered track state estimate of each filter model. Table 3 provides the peak RMS position and velocity errors for 10 selected periods of the target and sensor combinations. The target and sensor combination for each period is listed in the first two columns of Table 3.

The first two rows of Table 3 show the peak RMS errors of each filter model on the nonmaneuvering period of a target model. The scan sensor was the measurement source for period 1, and the HP sensor was the measurement source for period 2. Examination of the table entries shows that each of the IMM models outperforms the single filter models. This finding indicates that the proper model of each IMM, the CV with low process noise, was primarily selected for the nonmaneuvering trajectory. The single CV filter model could not achieve the same variance reduction on nonmaneuvering tracks as the IMM filters because the q value was selected high to limit lags on target maneuvers. The single CA filter model has the largest position and rate errors. Since the majority of most track periods in practical applications are nonmaneuvering, that would make this filter model undesirable.

The third row of Table 3 shows the peak RMS errors for the weaving target. None of the filter models selected for the IMM methods is matched to the changing dynamics of the weaving target. Thus, the results for this target do not show a clear advantage of one filter model over any of the others. Figure 2 shows the RMS velocity errors for all filter models as a function of time for the weaving target. This plot shows the relative performance of each filter model during the nonmaneuvering period (<60 s), as well as the magnitude of the errors during the weave. Although the IMM does not reduce errors during the weaving period, the performance is not degraded from any single model. Figure 3 shows

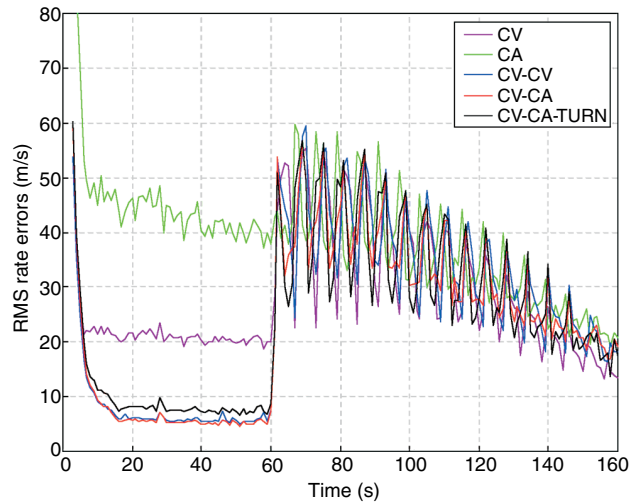


Figure 2. The filtered RMS velocity errors for the weaving target plotted as a function of time for each of the five filtering methods. Note that the weave maneuver begins at 60 s.

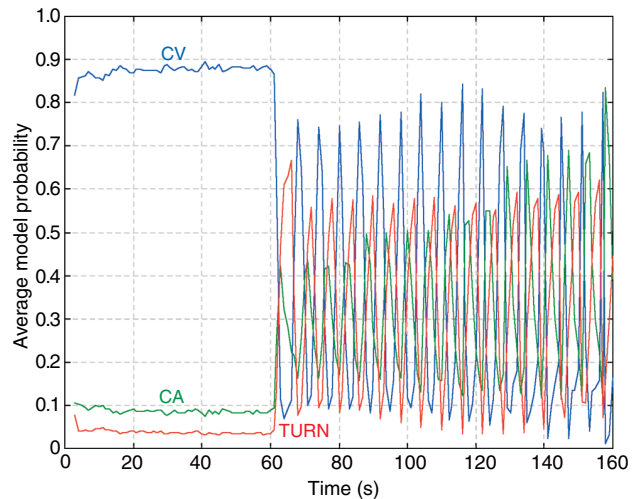


Figure 3. The average model probabilities for the CV-CA-TURN IMM on the weaving target. The model probabilities are averaged over 100 Monte Carlo realizations.

Target	Sensor	Position errors (m)/Velocity errors (m/s)				
		CV	CA	CV-CV	CV-CA	CV-CA-TURN
No maneuver	Scan	289/42	360/133	243/20	233/17	241/22
No maneuver	HP	50/23	59/49	40/10	34/7	36/9
Weave	HP	51/55	44/60	54/60	49/56	48/57
10-g acceleration	HP	64/112	37/64	37/73	43/76	44/80
Diver	Scan	246/206	180/136	175/154	172/132	167/129
Diver	HP	48/73	36/45	36/56	36/44	34/41
1-g turn	HP	85/36	100/63	86/39	85/47	81/36
5.6-g turn	Scan	968/323	445/179	432/188	444/174	391/120
5.6-g turn	HP	107/105	77/60	78/84	76/67	65/38
5.6-g turn (post maneuver)	HP	70/25	70/67	66/32	63/32	66/53

the average model probabilities for the CV-CA-TURN IMM on the weaving target. The CV model is dominant during the nonmaneuvering period, but the IMM algorithm is not able to find a single preferred model during the target weave.

The fourth row of Table 3 shows the peak RMS errors for the 10-g linear speed acceleration. This target maneuver should be well matched to the CA filter model. However, the results indicate that the single CA is only marginally better than the CV-CV IMM filter model. In addition, it appears that the CV-CV filter is better than the more complex CV-CA and CV-CA-TURN filter models. This is a deceptive result because the peak of the filter error is in the initial maneuver transition period. Figure 4 shows the RMS velocity errors as a function of time. This plot shows that although the errors at the start of the maneuver are similar, the CA, CV-CA, and CV-CA-TURN filters are much better in steady state. The plot also shows that the CA filter is slow to recover nonmaneuvering error levels after the maneuver ends. Thus, the additional filter models in the more complex filtering methods allow for a quicker recovery from the initial lag.

The fifth and sixth rows of Table 3 show the peak RMS errors for the high-altitude diving target using each sensor model. The results show a marginal improvement in the filter errors as the model complexity increases. Figure 5 shows the RMS velocity errors as a function of time for the diving target using the HP sensor model. This plot shows the peak errors at the start of the maneuver with the CV-CA-TURN IMM as best in steady state. This demonstrates that the TURN model implemented for this comparison study works well for maneuvers in three dimensions.

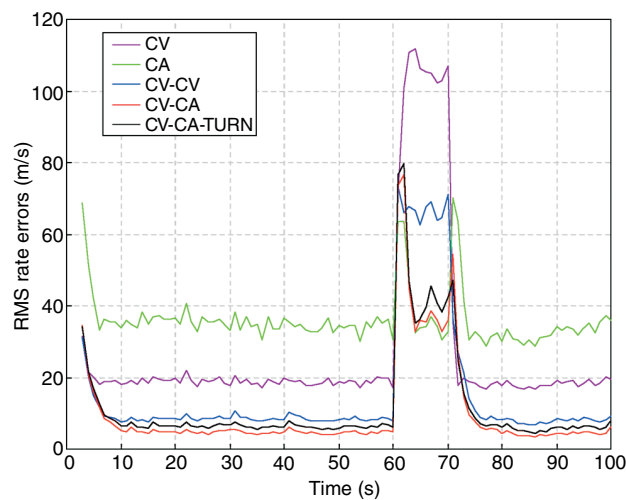


Figure 4. The filtered RMS velocity errors for the 10-g linear-speed accelerating target plotted as a function of time for each of the five filtering methods. Note that the maneuver occurs from 60 to 70 s.

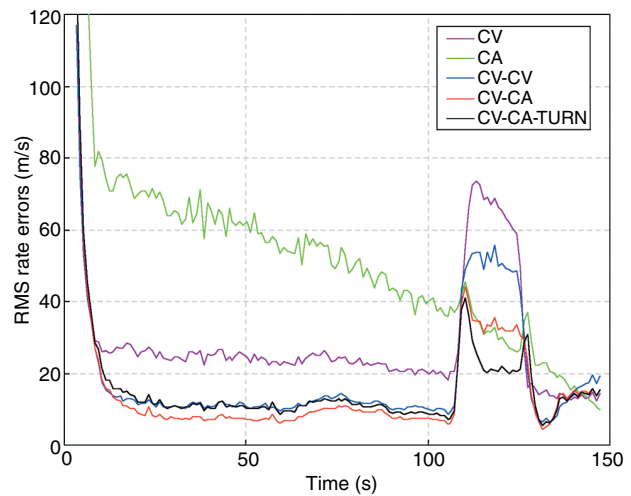


Figure 5. The filtered RMS velocity errors for the high-altitude diving target plotted as a function of time for each of the five filtering methods. Note that the dive starts at 110 s.

The seventh row of Table 3 shows the peak RMS errors for the 1-g constant-speed turn maneuver. All filter methods yield similar errors, with the exception of the single CA model, which had the worst overall performance. The lag errors produced from a small maneuver do not require the dynamic filter adaptability of a complex IMM. The errors did increase from the nonmaneuvering steady-state values, indicating that the IMM did detect the maneuver and adapt.

The eighth and ninth rows of Table 3 show the peak RMS errors for the 5.6-g constant-speed turn maneuver using each sensor model. The errors for these cases show a significant improvement as filter model complexity increases. This is expected since the TURN model is matched to the target maneuver. This is also true when either sensor was used to provide measurements to the filter models. Figure 6 shows the RMS velocity errors as a function of time for the 5.6-g turn using the HP sensor model. This plot confirms the error reduction achieved in the maneuver steady state using the CV-CA-TURN filter model. Note from Figure 6 the improvement from the CV-CV filter to the CV-CA filter model. This plot shows the short-duration increase in errors following the target maneuver for the CA and CV-CA-TURN models. The peaks of these errors are reflected in row 10 of Table 3. Shown in Figure 7 are the average model probabilities for the CV-CA-TURN IMM on the 5.6-g constant-speed turning target. These model probabilities reflect the correct selection of each filter model for the target duration that yielded the best overall error performance.

In general, the filter performance improved, with respect to RMS errors, as the complexity of the filter models increased. The CV filter model could not achieve the same variance reduction on nonmaneuvering tracks as the IMM filters because its q value was selected high

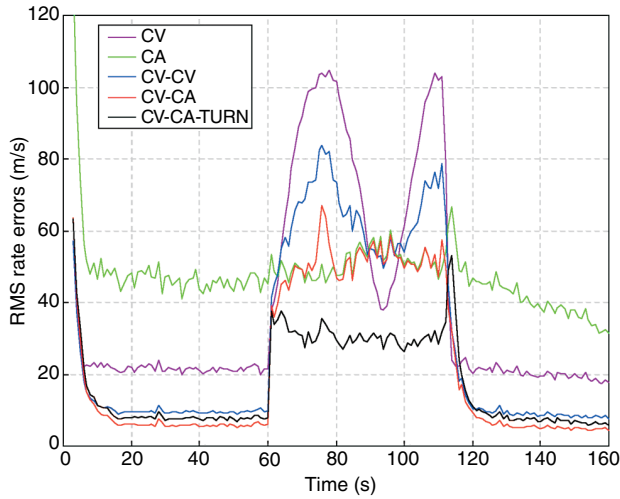


Figure 6. The filtered RMS velocity errors for the 5.6-g constant-speed turning target plotted as a function of time for each of the five filtering methods. Note that the turn maneuver occurs from 60 to 110 s.

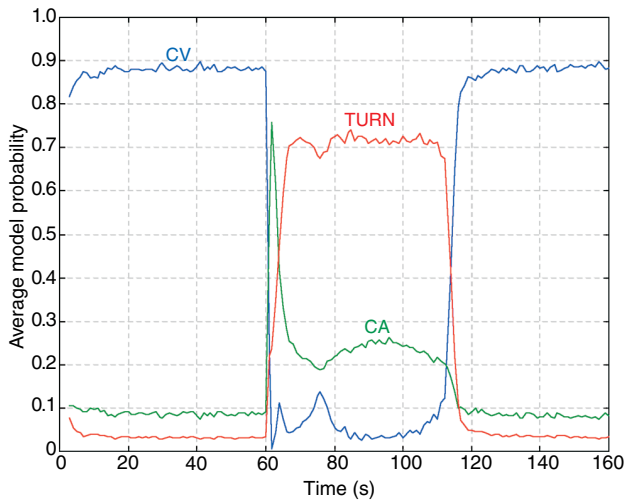


Figure 7. The average model probabilities for the CV-CA-TURN IMM on the 5.6-g constant-speed turning target. The model probabilities are averaged over 100 Monte Carlo realizations.

to limit lags on target maneuvers. However, this model also proved to have the largest errors during most of the target maneuvers. The CA model performed well with the target maneuvers but had the worst performance on the nonmaneuvering tracks.

All of the IMM models were equally effective on nonmaneuvering tracks. The key to the IMM filter model performance during target maneuvers is a match of the filter state models to the target dynamics. The CV-CV IMM does not try to model target maneuvers but instead limits lags by increasing filter gains. Thus this model had the largest errors of the IMM models during target maneuvers. The CV-CA IMM outperformed the CV-CV IMM on most target maneuvers because of the acceleration estimates in the filter model.

The CV-CA-TURN yielded the best overall performance on the turning targets while providing a comparable performance on all other targets.

PARAMETER SELECTION FOR THE IMM FILTER

Design parameters for the IMM filters are selected to control filter operating characteristics such as gain and response to maneuvers. The required design parameters for the filtering methods defined in the performance comparison are the IMM state switching matrix (Π) and the filter model q values.

State Switching Matrix

The state switching matrix is selected as part of the IMM algorithm to govern the underlying mode switching probabilities. This matrix defines the probability that a target will make the transition from one filter model state to another state. An example of a typical state switching matrix, for an IMM with two models, is given here:

$$\Pi = \begin{bmatrix} p^{11} & p^{12} \\ p^{21} & p^{22} \end{bmatrix} = \begin{bmatrix} 0.95 & 0.05 \\ 0.12 & 0.88 \end{bmatrix}.$$

The first filter model within an IMM is typically selected to handle the nonmaneuvering periods of a target trajectory. Under most conditions, this is best represented by a constant-velocity filter model with small process noise. As a general guideline, the first model is selected to have the highest probability. The second model, representing a target maneuver, is selected to be less probable than the first model. This is done to represent the behavior of typical airborne tracks.

Figure 8 shows the RMS velocity errors using the CV-CA IMM filter with three different state switching

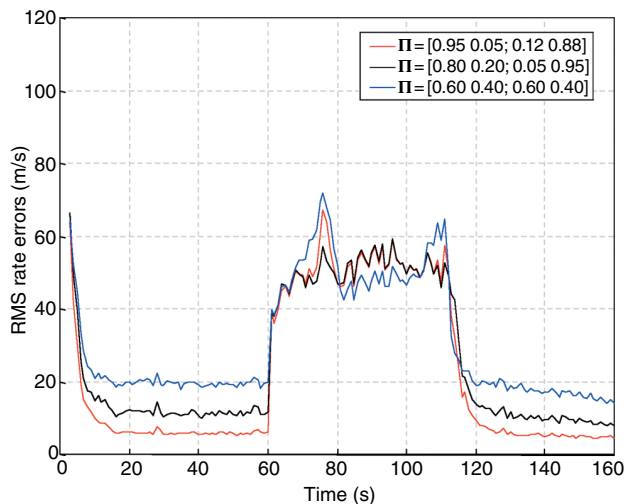


Figure 8. The filtered RMS velocity errors using a CV-CA IMM filter model with three different switching matrices plotted as a function of time using the 5.6-g constant-speed turning target.

matrices. The red curve represents the state switching matrix selected for the filter performance comparison study. A comparison of the plots of Figs. 6 and 8 shows that the selection of the filter models has a larger effect on state errors than subtle variations in the switching matrix. The black and blue curves in Fig. 8 show that moderate changes to the state switching matrix will effect small changes to the filter performance. The largest effects are seen during the nonmaneuvering periods when the total error is dominated by state noise. In general, the performance of the IMM appears to be relatively insensitive to the selection of the state switching matrix.

Process Noise Selection

The filter models defined for the filter performance comparison use process noise as a selected filter input to control the steady-state gains. The process noise is defined by a single selectable parameter specified as the q value. The relationship between the q value and steady-state Kalman filter gains is known. Reference 9 provides closed form expressions for the CV process noise model. Small q values yield small gains that provide good measurement noise reduction but lead to large lags during maneuvers. Large gains provide little noise reduction but give a better lag response during maneuvers. Conceptually, a multiple model filter algorithm could use two filters, one at each extreme of the gain spectrum, and the algorithm would select the proper balance between the two filters. This is not true for the IMM because selection of process noise needs to consider the interaction between filter models.

Mixing filter model states and covariances in the IMM algorithm allows for a prompt reaction to changing target modes. However, this mixing will also affect the individual filter model gains. An example of this effect is shown in the plots of Figs. 9 and 10. Figure 9 shows the bearing position gain as a function of time on a nonmaneuvering target for a single CV filter. Four curves are shown, representing different levels of input process noise. This plot shows reduction of the filter gain as q values are decreased. The plot in Fig. 10 shows the same curves taken from the first filter of a CV-CV IMM where the process noise of the second filter was kept constant. In contrast to the plot in Fig. 9, the gains in this plot are shown to reach a practical floor as the process noise is decreased. This floor varies with the q values of the second filter, indicating an inherent limitation in the realizable dynamic range of gains in a two-model IMM.

The IMM model probability calculations are affected by the process noise selection for each filter. The selection of process noise parameters for filters within the IMM requires a balance between the high and low models to achieve the best model interaction. When the difference between process noise in the two models

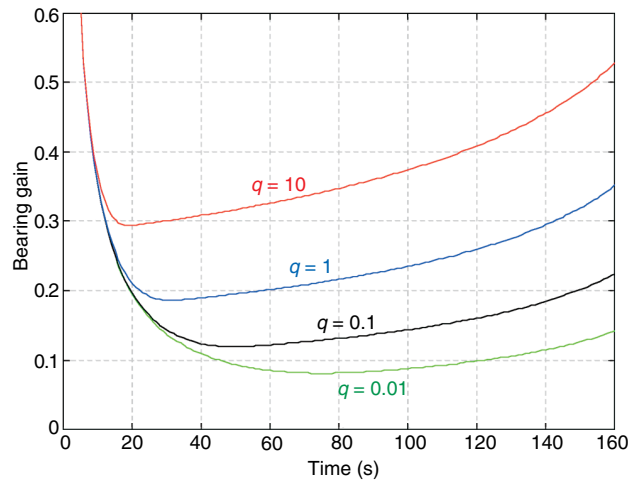


Figure 9. Single CV Kalman filter bearing position gains as a function of time on a nonmaneuvering target. The four curves represent different levels of input process noise.

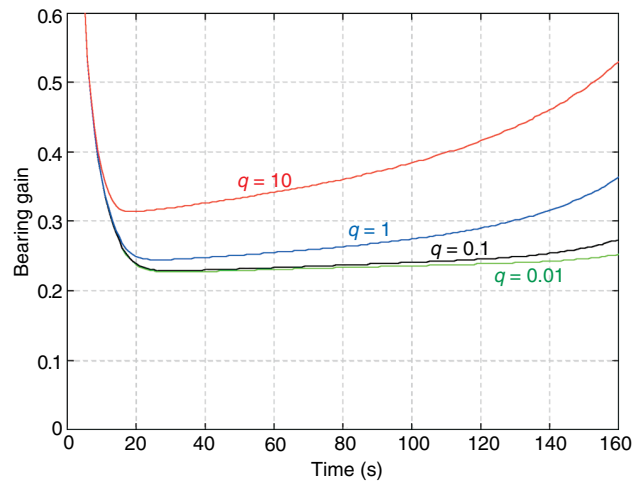


Figure 10. The bearing position gains for the first filter model from a CV-CV IMM plotted as a function of time on a nonmaneuvering target. The four curves represent different levels of input process noise on the first filter model. The q value for the second filter model was kept fixed at $15,000 \text{ m}^2/\text{s}^3$.

is too large, the probability of the maneuver model will be low during target maneuvers. The effect of this is a degraded performance on maneuvering targets when a filter with a higher process noise is used. Figure 11 shows RMS velocity errors from a CV-CV IMM filter model with three sets of q values. The plot represented by the red curve has the worst lag error during the target maneuver even though the process noise for the maneuvering model is the largest. Of note, the blue curve in Fig. 11 uses the same parameters from the filter comparison also plotted in Fig. 6. Similar to the state switching matrix, selection of the filter models has a larger impact on model performance than the selection of filter process noise.

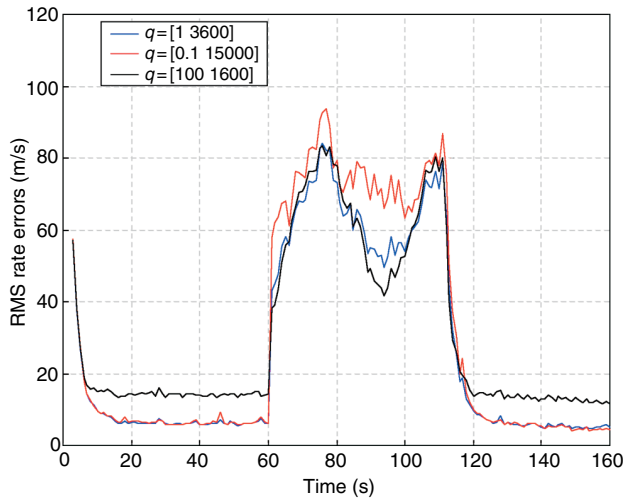


Figure 11. The filtered RMS velocity errors using a CV-CV IMM filter model with three different sets of input process noise plotted as a function of time for the 5.6-g constant-speed turning target.

CONCLUSIONS

The comparative results for five filter models on a variety of maneuvering targets show that methods that use the IMM algorithm provide the best overall results with respect to filtered position and rate errors. The performance improvement of the IMM is dependent on having filter models that are well matched to the target behavior. The filter model that is best matched to the target dynamics will provide the best state estimates and will have the highest probability. Results presented here also show that behavior of the IMM algorithm is robust when none of the filter models matches the target dynamics. The overall IMM performance will at

all times be similar to the best individual filter model within the IMM.

The performance of the IMM algorithm has been shown to be relatively insensitive to state switching matrix and filter process noise parameter selection. Results indicate that variations in the model parameters will effect small changes in the performance of the filter algorithm. Parameter selection needs to be considered to optimize the performance of an IMM given the component filter models. Selection of the component filter models should be the primary consideration for design of an IMM since the best overall performance is achieved when a filter model is matched to the target kinematics.

REFERENCES

- ¹Bar-Shalom, Y., Chang, K. C., and Blom, H. A. P., "Tracking a Maneuvering Target Using Input Estimation Versus the Interacting Multiple Model Algorithm," *IEEE Trans. Aerosp. Electronic Syst.* **EAS-25**(2), 296–300 (1989).
- ²Blackman, S. S., and Popoli, R., *Design and Analysis of Modern Tracking Systems*, Artech House, Norwood, MA, pp. 221–240 (1999).
- ³Yeddapanudi, M., Bar-Shalom, Y., and Pattipati, R., "IMM Estimation for Multitarget-Multisensor Air Traffic Surveillance," *Proc. IEEE* **85**(1), 80–94 (1997).
- ⁴Brown, R. G., and Hwang, P. Y. C., *Introduction to Random Signals and Applied Kalman Filtering*, Wiley, New York, pp. 230–236 (1992).
- ⁵Castella, F. R., "Multisensor, Multisite Tracking Filter," *IEE Proc. Radar, Sonar Navigation* **141**(2), 75–82 (Apr 1994).
- ⁶Castella, F. R., *Upgrading to a 9-State EKF for TBM Tracking*, F2A-96-0-021, JHU/APL, Laurel, MD (9 May 1996).
- ⁷Blair, W. D., Watson, G. A., and Alouani, A. T., *Use of Kinematic Constraint for Tracking Constant Speed Maneuvering Targets*, NAVSWC TR 91-561, Naval Surface Warfare Center, Dahlgren, VA (1991).
- ⁸Watson, G. A., and Blair, W. D., "IMM Algorithm for Tracking Targets That Maneuver Through Coordinated Turns," *SPIE—Signal and Data Processing of Small Targets* **1698**, 236–247 (1992).
- ⁹Ekstrand, B., "Analytical Steady State Solution for a Kalman Tracking Filter," *IEEE Trans. Aerosp. Electronic Syst.* **AES-19**(6), 815–819 (1983).

THE AUTHOR



ANTHONY F. GENOVESE is a member of APL's Senior Professional Staff. He received a B.S. in electrical engineering from Drexel University in 1992 and an M.S. in electrical engineering from The Johns Hopkins University Whiting School of Engineering in 1995. Since joining APL in 1992, his work has focused on development and testing of tracker algorithms for a variety of projects, including the Mk 92 Radar Processor, the Cooperative Engagement Capability, and the Italian Navy Archoboleno Program. Mr. Genovese is currently a member of the Sensor Signal and Data Processing Group of the Air Defense Systems Department. His e-mail address is anthony.genovese@jhuapl.edu.